Harnessing optogenetics to probe sub-cellular mechanics

Patrick W. Oakes[1,4*], Elizabeth Wagner[2*], Christoph A. Brand[3+], Dimitri Probst[3+], Marco Linke[3+], Ulrich S. Schwarz[3*], Michael Glotzer[2*], Margaret L. Gardel[1*]

[1]Institute for Biophysical Dynamics, James Franck Institute and the Department of Physics, University of Chicago, Chicago, IL 606037

[2]Department of Molecular Genetics and Cell Biology, University of Chicago, Chicago, IL 60637

[3]Institute for Theoretical Physics and BioQuant, Heidelberg University, Heidelberg, Germany

[4]Department of Physics & Astronomy, and Department of Biology, University of Rochester, Rochester, NY 14627

[*,+]Contributed equally

[*]Corresponding Authors

1 **Abstract**

2 The mechanics of the actin cytoskeleton regulates cell morphogenesis during essential physiological

3 processes. However, the spatially heterogeneous and dynamic nature of the actin cytoskeleton make

4 mechanical measurements and modeling challenging. Here we develop a new approach to probe the

5 mechanics of the contractile actin cytoskeleton by integrating optogenetic control of RhoA, live cell

6 imaging and traction force microscopy. Local activation of RhoA stimulates local contraction, leading to

7 increased traction forces that rapidly propagate across the cell via stress fibers and drive actin flow

8 towards the region of heightened RhoA. Surprisingly, the flow reverses direction when local RhoA

9 activation stops. These experimental data are used to constrain a physical model, which demonstrates

10 that stress fibers are elastic-like, even at time scales exceeding turnover of constituent proteins. We

11 identify zyxin as a regulator of stress fiber mechanics, as they are fluid-like in its absence. Such

12 molecular control of actin mechanics likely plays critical roles in regulation of morphogenic events.

13   **Introduction**

14   A diverse array of essential physiological processes, ranging from the subcellular to the multicellular,

15   depend on the spatial and temporal regulation of contractile forces[1-4]. This regulation drives changes in

16   cell shape[5,6] and mediates interactions with the extracellular environment [7,8]. Changes in contractility

17   can furthermore alter gene expression[9] and impact development[10,11]. The molecular machinery

18   required for generating contractile forces is well conserved and dominated by the actin cytoskeleton,

19   myosin II activity and associated regulatory proteins[4,12,13]. Specifically, actin filaments dynamically

20   organize into distinct contractile architectures, including the cortex and stress fibers [14,15]. Contractile

21   forces are transmitted across the cell by actin arrays and are ultimately to the extracellular matrix by

22   focal adhesions[12,13,16,17].

23

24   The regulation of cellular force transmission is controlled by the mechanical properties of actomyosin

25   assemblies. Cellular mechanics has been explored extensively both experimentally[14,18-20] and

26   theoretically[21-23]. Current understanding is that, at time scales comparable to those of typical kinetic

27   processes, the actin cytoskeleton behaves like an elastic solid. Such elasticity enables rapid force

28   transmission across the cell and reversible deformations to preserve cytoskeletal architecture. In

29   contrast, at longer time scales, it is thought dynamic processes make the cytoskeleton predominately

30   like a viscous fluid. Such viscosity enables cytoskeletal flows and remodeling. However, the molecular

31   regulation of cell mechanics is not well understood.

32

33   Cellular contractility is largely controlled by the activity of the small GTPase RhoA[24,25], which in

34   adherent cells is preferentially active at the cell periphery[26,27]. RhoA regulates contractility through the

35   promotion of actin polymerization and myosin light chain phosphorylation via the downstream

36   effectors Diaphanous-related formins and Rho-associated Kinase (ROCK), respectively. RhoA activity is

37   required for stress fibers and focal adhesions[24,25]. Little, however, is known about how small changes in

38   activity can regulate cell contractility, actin architecture and adhesion.

39

40   In this paper, we have used an optogenetic probe to locally activate RhoA in adherent fibroblasts.

41   Plasma membrane recruitment of the RhoA specific guanine exchange factor (GEF) LARG induces local

42   RhoA activation[6,28-30]. Local activation of RhoA leads to an increase in actin polymerization and myosin

43   activity in the region of activation, but it does not stimulate *de novo* stress fiber formation or changes

44   in focal adhesion morphology. We find that exogenous RhoA activation leads to an immediate increase

45   in both the local and global contractility of the cell, followed by a rapid relaxation after GEF

46   recruitment is stopped. The local increase in stress fiber contractility drives an actomyosin flow

47   towards regions of increased RhoA activity. Surprisingly, these flows reverse direction as soon as GEF

48   recruitment ceases. Using physical modeling, we show this behavior is consistent with stress fibers

49   behaving as predominately elastic-like over hour time scales. We find that zyxin is necessary for this

50   elasticity; in its absence, stress fibers become predominately fluid-like even at second time scales.

51   These results suggest that stress fiber mechanics is sensitive to small changes in composition, which

52   has significant implications for regulation of force transmission and cytoskeletal organization.

53

54   **Results**

55   **Spatiotemporal control of RhoA and its downstream effectors**

56   To spatially and temporally control contractility in adherent cells, we adapted a previously established

57   optogenetic probe[6,28] to act on the RhoA signaling pathway (Figure 1a). During stimulation by blue

58   light, a cytosolic fusion protein, photo-recruitable GEF (prGEF), consisting of tandem PDZ domains

59   fused to the DH domain of the RhoA specific GEF LARG[6], is recruited to the plasma membrane where it

60   activates RhoA (Figure 1b). To illustrate the local recruitment of prGEF we tagged it with the

61   fluorophore mCherry and imaged an NIH 3T3 fibroblast expressing the constructs on a glass coverslip

62   (Figure 1c). A digital micromirror device was used to spatially control the illumination of the blue

63   activating light (orange box, Figure 1c), and was pulsed before each image acquisition during the

64   recruitment period. Recruitment of the prGEF to the activation region was rapid and reversible upon

65   extinguishing the stimulating blue light (Figure 1c,d and Supplementary Movie 1).

66

67   To investigate whether recruitment of the prGEF resulted in activity of proteins downstream of RhoA,

68   we tracked the dynamics of actin and myosin light chain (MLC) during recruitment (Figure 1e,g). Both

69   actin and myosin accumulated in the activation regions, resulting in an increase in fluorescence

70   intensity during the 15 min activation period (Figure 1e-h and Supplementary Movies 2-3).

71 Interestingly, local activation of RhoA did not lead to *de novo* stress fiber assembly in the activation

72 region (Figure 1e and Supplementary Movie 2). At the end of the activation period, fluorescence

73 intensities of both actin and myosin returned to baseline levels. These results indicate that exogenous

74 RhoA activation via LARG recruitment is not sufficient to maintain elevated RhoA activity and the

75 concomitant increases in local actin and myosin concentrations. To confirm that local activation of

76 RhoA was acting on actin and myosin through its downstream effectors, formin and ROCK, the

77 experiments were repeated in the presence of either SMIFH2, a pan formin inhibitor[31], or Y-27632, a

78 Rho-associated Kinase inhibitor. Local recruitment of actin and MLC were significantly inhibited by the

79 presence of SMIFH2 and Y-27632, respectively. These results illustrate that RhoA activity and

80 recruitment of its downstream effectors can be spatially and temporally controlled via light.

81

82 **Focal adhesion dynamics and morphology are unperturbed by local increases in RhoA activity**

83 Previous work has suggested that focal adhesion formation and maturation are tension dependent

84 processes driven by increased RhoA activity at adhesion sites [24,25,32]. To test these hypotheses we

85 examined how local RhoA activation affected traction forces and focal adhesions. Cells expressing

86 mCherry-vinculin, a marker of focal adhesions, were plated on polyacrylamide gels coated with

87 fibronectin and traction stresses were measured via Traction Force Microscopy (Figure 2a,b and

88 Supplementary Movie 4)[33,34]. During local activation of RhoA, traction stresses increased at focal

89 adhesion sites, on a similar timescale to that of myosin localization (Figure 1g). Despite the increased

90 force, the total number of adhesions remained essentially constant (Figure 2c). Individual adhesion

91 morphology and vinculin intensity were also unaffected, despite large increases in stress at a majority

92 of previously established adhesion sites during local RhoA activation (Figure 2d & Supplementary

93 Figure S1). Too much RhoA activation, however, results in adhesion failure and detachment from the

94 substrate (Supplementary Figure S2). These result are consistent with previous results that tension

95 alone is not sufficient to drive changes in focal adhesion size[35].

96

97 To determine the effect of local RhoA activation on the overall contractility of the cell, we used traction

98 force microscopy to measure the total strain energy, which reflects the amount of mechanical work

99 done by the cell on its environment[36]. Activation induced a rapid increase in both traction stresses and

5

100   strain energy (Figure 2b,c) At the end of the activation period, the strain energy decreased to their

101   original baseline values (Figure 2c). Interestingly, traction stresses were mostly seen to increase at the

102   cell periphery, where traction stresses were already established, and in areas immediately adjacent to

103   the activation region. No change was seen in the activation area itself (Figure 2b). This suggests that

104   locally generated forces balance within the activation region and only unbalanced forces at the edge of

105   this region are turned into productive traction forces. Thus, a local increase of tension leads to globally

106   distributed traction forces at pre-existing focal adhesions.

107

108   **Cells maintain a contractile set point**

109   That cells return to a similar baseline contractility following a period of exogenous RhoA activation is

110   consistent with previously established ideas of tensional homeostasis[36-38]. To explicitly probe this

111   behavior, we performed a series of local activations of different sizes on a single cell (Figure 2e and

112   Supplementary Movie 5). After measuring the strain energy at an initial steady state, a cell was

113   exposed to three 15 min periods of local RhoA activation of increasing size with relaxation periods

114   between each activation (Figure 2e,f). The strain energy increased concomitant with the size of the

115   activation region. During activation, both local stresses immediately surrounding the activation region,

116   and long-range stresses at the cell periphery could be seen to increase (Figure 2e). Following each

117   activation, the strain energy returned to the initial baseline level (Figure 2f).

118

119   To elucidate the underlying mechanical principles, we built a physical model that would capture this

120   physical response. We constructed a continuum model of the cell as a contractile element in series

121   with a viscous and an elastic element (Figure 2g). Contractility was assumed to increase with an

122   exponentially plateauing ramp in the activated region, consistent with the observed accumulation

123   profiles for actin and myosin (Figure 1g), and the substrate was represented as an elastic spring

124   coupled to the cell by a friction element. The model parameters for the elastic modulus, viscosity,

125   friction and contractility were found by fitting the model to the strain energy data, while the value of

126   the substrate stiffness was fixed. This procedure resulted in a curve in good agreement with the

127   experimental data (Figure 2f).

128

129   We find that both the viscous and elastic elements are necessary to accurately capture the behavior of

130   the system. The ratio of viscosity (~7*10^6 Pa*s) to elasticity (~2*10^3 Pa) defines a viscoelastic

131   relaxation time of approximately 50 minutes; this time scale determines the transition from when the

132   cytoskeleton behaves predominately elastic-like (< 50 min) to predominately fluid-like (> 50 min). Our

133   results thus indicate that stress fibers are predominantly elastic on the scale of tens of minutes, despite

134   proteins within the stress fiber turning over on timescales of tens of seconds[15]. This strong elastic

135   behavior is also consistent with the immediate increase in cell traction stresses at the cell periphery

136   (Figure 2b,e) upon local activation of RhoA in the center of the cell.

137

138   **Stress fibers contract independent of the background network**

139   To investigate the cytoskeletal architectures that give rise to this strong contractility, we tracked

140   myosin dynamics during local RhoA activation. In the steady state, as new actomyosin is polymerized

141   and incorporated into stress fibers, there is a retrograde flow of actomoysin from the periphery

142   towards the cell center[15,17]. Using particle image velocimetry (PIV)[39,40] we measured both the local

143   direction and magnitude of myosin flow. We found that myosin flow rates along the stress fiber

144   increased as myosin accumulated in the activation region creating a local contraction, and that this

145   flow was directed along the orientation of the stress fibers spanning the activation region (Figure 3a,b,

146   Supplementary Figure S3, and Supplementary Movie 6). The flow direction was independent of the

147   activation region geometry, with the direction always being determined by the stress fiber orientation

148   (Supplementary Movie 7).

149

150   The cytoskeleton of a strongly adherent cell is typically thought to be a 2D material comprised of stress

151   fibers embedded in an isotropic cortex[34,41,42]. Since flows induced by local RhoA activation appear to

152   track the orientation of the stress fibers (Figs. 3a,b and S2), we sought to address the relative

153   contractile contributions of the stress fibers and the actin networks. We therefore built a 2D discrete

154   model analogous to the 1D continuum model described above (Figure 3c). The model consists of a

155   triangular mesh with the same contractile, viscous and elastic elements connected in series, with lines

156   of increased contractility representing the stress fibers. Using a simple rectangular cell, we first verified

157   that, without stress fibers, this model recapitulates the results from the one-dimensional continuum

7

158   model (Figure 3d). Similar to the 1D model above, the contractile components in a region in the center

159   of the cell were slowly increased with an exponentially plateauing ramp. The parameters were then

160   adjusted so that the model both qualitatively and quantitatively recapitulated the expected flow

161   patterns of the 1D continuum model (Figure 3d).

162

163   To explore the relative contributions of the background mesh and the stress fibers, we considered two

164   test cases: (1) If both the mesh and the stress fibers contained contractile elements, the stress fibers

165   pinched inward transverse to their orientation during local activation (Figure 3e); and (2) when

166   contractile elements were only included in the stress fibers, the cytoskeletal flow was restricted to

167   directions along the stress fiber (Figure 3f), consistent with our experimental results (Figure 3a-b,

168   Supplementary Figure S3, and Supplementary Movies 6-7). Since transverse deformations were never

169   seen in experiments, it is clear that the stress fibers must be the predominant contractile elements

170   observable at this resolution which respond to local RhoA-induced contractions. Furthermore, this

171   result illustrates that it is appropriate to think of a stress fiber as a one-dimensional contractile

172   element with viscous and elastic components embedded in a passive viscoelastic network.

173

174   **Stress fibers flow in response to local strain induced by RhoA activation**

175   Having identified the stress fiber as the main contractile unit responding to exogenous RhoA activation,

176   we next sought to address whether stress fibers undergo deformation during contraction. Since stress

177   fibers can be considered as 1D structures, we analyzed myosin flow along the fiber using kymographs.

178   A kymograph drawn along a single stress fiber illustrates that myosin puncta flowed from both ends

179   towards the activation regions when RhoA was activated locally (Figure 4a-b, Supplementary Figure

180   S5). Similarly, a kymograph drawn by projecting the flow speed along the stress fiber from the velocity

181   field created by our PIV analysis illustrates even more clearly how cytoskeletal flow was perturbed by

182   local RhoA activation. Flow of myosin from both ends of the stress fiber reoriented towards the

183   recruitment regions and increased from ~1 nm/s on average to more than 3 nm/s during activation

184   (Figure 4c and Supplementary Figure S5). Strikingly, the flow was also seen to reverse direction, flowing

185   away from the recruitment region and towards the cell periphery, during the relaxation period

186   following the local activation (Figure 4b,c). This flow reversal is reminiscent of the restoring force in

8

187   elastic objects that restores its original shape after removal of external force (e.g. recoil of an elastic

188   band after stretch).

189

190   We next developed a protocol to measure the magnitude of the stress fiber displacement during these

191   periods of contraction and relaxation (Figure 4d). The displacement in a given fiber was determined by

192   measuring the relative position of puncta along the fiber following 15 minutes of local RhoA activation

193   and 15 minutes after it ceased. During contraction, puncta on either side of the activation region

194   contracted on average ~3 μm from their original position before relaxing back to ~1 μm from their

195   original position (Figure 4d). The relaxation response across many stress fibers from multiple cells

196   could be further clustered into two groups, one which exhibited strong reversal (~80% of the original

197   position) and one which exhibited little to no reversal (~25% of the original position) (Figure 4d).

198

199   To determine whether stress fibers were stretching due to the local contraction, we used cells

200   expressing mApple-α-actinin, an actin crosslinker which localizes to well defined puncta on stress fibers

201   (Figure 4e and Supplementary Movie 8). We created kymographs of α-actinin flow during local

202   activation of RhoA and tracked paths of individual puncta (Figure 4f). The velocity of individual puncta

203   was determined from the slope of the tracks in the kymograph and plotted as a function of distance

204   from the activation zone (Figure 4g). Puncta along the stress fiber moved at similar speeds, indicating

205   that, in general, the stress fiber was translating as a rigid rod during the local contraction (Figure 4g).

206   Where present, changes in velocity between neighboring puncta were abrupt (blue arrow Fig 4g),

207   suggesting points of structural failure along a fiber. These results indicate that the strain induced in the

208   stress fiber is restricted to the local contraction in the activation region and discrete sites of extension

209   in regions outside the activation region.

210

211   By fitting the experimental kymographs to both our 1D continuum and 2D discrete models, we show

212   that similar flow patterns emerge naturally from the mechanics of the system (Figure 4h). The high

213   elasticity of the stress fiber, specifically the ratio of elasticity to viscosity, is sufficient to recapitulate

214   the flow profiles that were seen during both RhoA activation and relaxation. Furthermore, the

215 parameters found from the kymograph fitting process were consistent with the parameter values

216 found when fitting the strain energy (Table 2).

217

218 **Zyxin is recruited to sites of extension and compression on stress fibers**

219 In order to probe the underlying molecular basis of this elasticity, we sought to identify stress fiber-

220 associated proteins that could contribute to the recoil behavior. Zyxin has been previously established

221 as a mechanosensitive protein that dynamically localizes to sites of strain along stress fibers[43,44], in

222 addition to focal adhesions[45]. Using cells expressing mCherry-zyxin, we monitored zyxin activity during

223 RhoA activation (Figure 5a and Supplementary Movie 9). Zyxin recruitment was consistently observed

224 in a small population of focal adhesions outside of the local activation region (Figure 5b). Surprisingly,

225 we found that zyxin also accumulated along stress fibers in the region of local activation (Figure 5c,d).

226 Given the myosin accumulation and direction of flow, this suggests that zyxin is recruited to both sites

227 of compression and extension. Paxillin, another mechanosensitive LIM domain protein that responds

228 to stress [46,47], behaved similarly to zyxin (Supplementary Figure S4).

229

230 **Zyxin is required for stress fibers to behave elastically**

231 To further explore the role of zyxin in stress fiber mechanical behavior we used mouse embryonic

232 fibroblast cells derived from zyxin^{-/-} mice[48]. Despite the loss of zyxin, these cells form actin stress fibers

233 and focal adhesions and are highly contractile[49]. When we locally activated RhoA in the zyxin^{-/-} cells,

234 myosin accumulated in the activation region (Figure 5e and Supplementary Movie 10). This

235 accumulation drove a contractile flow into the local activation area that was indistinguishable from

236 wild type cells. Upon stopping the GEF recruitment in zyxin^{-/-} cells, cytoskeletal flow returned to pre-

237 activation rates, consistent with the reduced local contraction, but did not reverse direction (Figure 5e-

238 f,i, Supplementary Figure S5, and Supplementary Movie 10). Expression of EGFP-zyxin in this cell line

239 restored the flow reversal (Figure 5g-i, Supplementary Figure S5 and Supplementary Movie 11).

240 Together these results indicate that zyxin is required for the flow reversal occurring after local RhoA

241 activation ends.

242

10

243 Using the kymographs produced in the zyin^{-/-} and zyxin^{-/-}+EGFP-zyxin cells, we again fit the data to our

244 mechanical model (Figure 5j-l, Supplementary Figure S6). For the zyxin^{-/-} cells, we found the viscoelastic

245 relaxation time reduced to 1 sec, indicating that the stress fibers are predominately fluid-like at all

246 physiological time scales. Rescue of the zyxin^{-/-} cells with EGFP-zyxin resulted in parameter fits that

247 were consistent with the NIH 3T3 fibroblast data. Zyxin is thus important for maintaining the

248 qualitative mechanical response of stress fibers, ensuring they are predominately elastic at ~1 hr time

249 scales.

250

251 **Discussion**

252 This study demonstrates that the mechanical behavior of adherent cells is strongly shaped by stress

253 fibers and their ability rapid force transmission and cytoskeletal architecture even in the face of

254 molecular turnover and flow. Using an optogenetic probe to locally activate RhoA via recruitment of

255 the DH domain of LARG, a RhoA specific GEF, we find that we can stimulate a local contraction in stress

256 fibers due to an increased accumulation of actin and myosin in the activation area (Figure 6, 1). This

257 local contraction causes a tension gradient and a flow towards the activation region (Figure 6, 2). The

258 flow of myosin and α-actinin increases the strain both on the interface coupling the stress fiber to the

259 adhesion and in the activation region, leading to recruitment of the mechanosensitive protein zyxin

260 (Figure 6, 3). When local activation of RhoA is stopped, the system relaxes to the pre-activation state,

261 mainly driven by elastic energy accumulated in the strained regions, and results in a cytoskeletal flow

262 of material away from the local activation region (Figure 6, 4).

263

264 This elastic behavior is dependent on zyxin. Previous reports have shown that zyxin localizes along the

265 stress fiber at the interface of the adhesion[50,51]. This positioning suggests that previously reported

266 zyxin mediated stress fiber repair mechanisms[46,49] are also occurring at the adhesion interface as actin

267 is assembled and is incorporated into the stress fiber while under tension. The localization of zyxin to

268 sites of compression, however, is novel. While it is known that the LIM domain of zyxin is sufficient for

269 localization[52], the exact mechanism through which zyxin recognizes sites of strain remains unknown.

270

11

271   These data further illustrate that RhoA activity and its downstream effectors are tightly regulated by

272   the cell. We see no evidence that RhoA activation alone leads to *de novo* stress fiber formation or

273   adhesion maturation. Instead these processes likely result from concurrent changes in cytoskeletal

274   architecture[35,53]. More interestingly, the data suggest cells regulate total RhoA activity to maintain a

275   constant homeostasis[36-38]. Specifically, the relaxation kinetics of the downstream effectors match the

276   kinetics of the optogenetic probe[28], thus indicating that there is no positive feedback loop whereby

277   production of RhoA•GTP alone is sufficient to promote further activation of RhoA. To sustain a given

278   contractile state, therefore, the cell must actively regulate and maintain a specific RhoA•GTP

279   concentration.

280

281   By using an optogenetic approach to perturb the local mechanical balance within the cell, we were

282   able probe the material properties of the cytoskeleton in ways previously inaccessible. Given that

283   typical turnover rates for proteins in the cytoskeleton are on the order of tens of seconds[15], it is

284   surprising that the cell behaves elastically on timescales of ~1 hour. The viscous behavior of cells is

285   typically associated with irreversible changes brought on through remodeling and dynamic activity of

286   proteins (e.g. cytoskeletal remodeling during migration)[21,54,55]. Conversely, elasticity has typically been

287   used to describe cellular material properties that ignore the dynamic activity of the components[36,56,57].

288   The finding that cells can maintain their elasticity and their dynamic activity simultaneously has

289   exciting implications for interpreting the underlying physics of active materials. The fact that this

290   behavior can be controlled by the activity of a single protein suggests intriguing potential mechanisms

291   to regulate cell mechanics during morphogenesis and development.

292   **Methods**

293   **Cell culture and transfection**

294   NIH 3T3 fibroblasts (American Type Culture Collection, Manassas, VA) were cultured in DMEM media

295   (Mediatech, Herndon, VA) and supplemented with 10% FBS (HyClone; ThermoFisher Scientific,

296   Hampton, NH), 2 mM L-glutamine (Invitrogen, Caarlsbad, CA) and penicillin-streptomycin (Invitrogen).

297   Zyxin^{-/-} and zyxin^{-/-}+EGFP-zyxin Mouse Embryonic Fibroblast cells were a gift of Mary Beckerle's lab

298   (University of Utah, Salt Lake City, UT) and cultured similarly to the NIH 3T3 fibroblasts[49]. All cells were

299   transiently transfected via electroporation 24 hrs prior to experiment using a Neon Transfection

300   system (ThermoFisher Scientific). Following transfection, cells were plated on glass coverslips and

301   imaged the next day.

302

303   **Drug treatments**

304   Cells were treated with either the 10 μM SMIFH2 a pan-formin inhibitor[31] or 1μM of Y-27632 which

305   inhibits ROCK (ThermoFisher Scientific), for at least 30 minutes prior to imaging.

306

307   **Plasmids**

308   The optogenetic membrane tether consisting of Stargazin-GFP-LOVpep and prGEF constructs used are

309   previously described (Wagner 2016). prGEF-YFP was constructed in an identical manner to prGEF with

310   YFP replacing mCherry. This construct was used in experiments where the effects on various

311   downstream markers were visualized. To examine effects on the actin and myosin networks, we used

312   mApple-Actin and mApple-MLC constructs (gifts from M Davidson, University of Florida, Gainesville FL),

313   mCherry-Vinculin (gift from V Weaver, University of California at San Francisco, San Francisco, CA) and

314   mCherry-zyxin (gift from M Beckerle, University of Utah, Salt Lake City, UT).

315

316   **Live cell imaging**

317   Glass coverslips were placed in a Chamlide magnetic chamber (Live Cell Instrument, Seoul, Korea) in

318   culture media supplemented with 10 mM HEPES and 30μL/mL Oxyrase (Oxyrase Inc., Mansfield, OH)

319   and maintained at 37˚C. Cells were imaged on an inverted Nikon Ti-E microscope (Nikon, Melville, NY)

320   with a Yokogawa CSU-X confocal scanhead (Yokogawa Electric, Tokyo, Japan), and laser merge module

13

321   containing 491nm, 561nm, and 642nm laser lines (Spectral Applied Research, Ontario, Canada). Images

322   were collected on either a CoolSNAP HQ2 CCD (Roper Scientific, Trenton, NJ) or Zyla 4.2 sCMOS

323   Camera (Andor, Belfast, United Kingdom). Local recruitment using the optogenetic probe was

324   performed using a 405 nM laser coupled to a Mosaic digital micromirror device (Andor). Images were

325   collected using a 60x 1.49 NA ApoTIRF oil immersion objective (Nikon). All hardware was controlled

326   using MetaMorph Automation and Image Analysis Software (Molecular Devices, Sunnyvale, CA).

327

328   Unless otherwise stated, cells were imaged in the 561 channel every 20 s for 45 min, with the first 15

329   min used to determine the steady state of the system, the second 15 min to perform local recruitment,

330   and the final 15 min to record any recovery. During recruitment a local region drawn in MetaMorph

331   was illuminated by the 405nm laser for 960 ms at a power < 1 μJ/s immediately prior to the acquisition

332   of each 561 image.

333

334   **Local recruitment analysis**

335   All data analysis was performed using MATLAB (Mathworks, Natick, MA). Regions of interest (ROIs)

336   were drawn to calculate the average intensity in the local recruitment region, a control area within the

337   cell but far away from the recruitment area, and a background area outside of the cell. The average

338   background intensity was subtracted from the control region and this curve was used to determine a

339   photobleaching correction. The photobleaching correction was then applied to the background

340   subtracted average intensity in the local recruitment region and normalized to the average value of the

341   first 15 min of the data.

342

343   **Focal adhesion analysis**

344   Images were thresholded and segmented to create binary masks using MATLAB. Adhesion masks were

345   filtered to exclude adhesions smaller than 0.4 μm^2 due to the inability to segment them consistently.

346   The binary mask was then used to calculate the total number and average fluorescence intensity of

347   adhesions in each frame. These masks were also used to calculate the average stress under the

348   adhesions. To calculate the percentage of adhesions which increased in intensity or stress during

349   activation, we compared the maximum intensity of the adhesion during activation to the intensity

14

350 immediately prior to activation. Adhesions were considered to have shown an increase in either

351 intensity or stress if the magnitude of the increase was greater than 10%.

352

353 **Kymograph and local displacement analysis**

354 Kymographs were created in MATLAB by drawing lines along stress fibers and averaging across a width

355 of 9 pixels. Local displacement was determined by locating a feature 5μm from the edge of the

356 activation zone in a kymograph immediately prior to activation. The location of this feature was then

357 tracked and recorded following the 15 minute period of activation, and then again following 15

358 minutes of relaxation.

359

360 **Cytoskeletal flow analysis**

361 Images were first corrected for bleaching and then filtered with a 3D Gaussian filter to remove noise.

362 Flow fields were calculated using an implementation of the Brox et al. optical flow algorithm[39,40] that

363 ensures spatial and temporal smoothness. Flow field kymographs were generated by projecting the

364 flow vectors onto the line defining the kymograph. To compare the direction of flow with the

365 organization of the cytoskeleton, the local orientation of actin fibers was extracted from the structure

366 tensor[58].

367

368 **α-actinin spacing analysis**

369 Kymographs were drawn as above. For each timepoint in the kymograph, local peaks in the linescan

370 were determined. Peaks were then connected to create tracks across the kymograph. Local velocity

371 was determined by isolating the section of the track during the activation period and fitting the

372 trajectory to a straight line. The fitted slope was taken as the velocity.

373

374 **Traction force microscopy**

375 Traction force microscopy was performed as described previously[33,34,36]. Briefly, polyacrylamide gels

376 embedded with 40-nm fluorescent microspheres (Invitrogen) were polymerized on activated glass

377 coverslips. The shear modulus of the gels used in these experiments was 8.6 kPa. Following

378 polymerization gels were washed with PBS and crosslinked with the extracellular matrix protein

379 fibronectin (Millipore, Billerica, MA) using the photoactivatable crosslinker sulfo-sanpah (Thermo

380 Fisher Scientific). Cells were plated and allowed to spread for at least 4 hours prior to imaging as

381 described above.

382

383 Following imaging, cells were removed from the substrate using 0.5% sodium dodecyl sulfate and a

384 reference image of the fluorescent beads in the unstrained substrate was taken. The image stack was

385 then aligned to correct for drift and compared to the reference image using particle imaging

386 velocimetry to create a displacement field with a grid spacing of 0.86 μm. Displacement vectors were

387 filtered and interpolated using the Kriging interpolation method. Traction stresses were reconstructed

388 via Fourier Transform Traction Cytometry[33,59], with a regularization parameter chosen by minimizing

389 the L2 curve[34]. The strain energy was calculated as one half the integral of the traction stress field

390 dotted into the displacement field[36].

391

392 **Statistical analysis**

393 All experiments were repeated a minimum of 3 times. Cells presented in figures are representative

394 samples of the population behavior. Box plots represent the 25th, 50th and 75th percentiles of the data.

395 Whiskers on the boxplot extend to the most extreme data points not considered outliers. Error bars

396 represent the standard deviation, except where noted otherwise. Statistical significance was

397 determined using independent two-sample Student's *t* tests of the mean to compare groups of data.

398 Statistical significance is indicated by asterisks: (*) represents a *p*-value < 0.05; (**) represents a *p*-

399 value < 0.01.

400

References:

1. Lecuit, T., Lenne, P.-F. & Munro, E. Force generation, transmission, and integration during cell and tissue morphogenesis. *Annu Rev Cell Dev Biol* **27,** 157–184 (2011).

2. Paluch, E. & Heisenberg, C.-P. Biology and Physics of Cell Shape Changes in Development. *Current Biology* **19,** R790–R799 (2009).

3. Iskratsch, T., Wolfenson, H. & Sheetz, M. P. Appreciating force and shape—the rise of mechanotransduction in cell biology. *Nat Rev Mol Cell Biol* **15,** 825–833 (2014).

4. Murrell, M., Oakes, P. W., Lenz, M. & Gardel, M. L. Forcing cells into shape: the mechanics of actomyosin contractility. *Nat Rev Mol Cell Biol* **16,** 486–498 (2015).

5. Martin, A. C., Gelbart, M., Fernandez-Gonzalez, R., Kaschube, M. & Wieschaus, E. F. Integration of contractile forces during tissue invagination. *J Cell Biol* **188,** 735–749 (2010).

6. Wagner, E. & Glotzer, M. Local RhoA activation induces cytokinetic furrows independent of spindle position and cell cycle stage. *J Cell Biol* **213,** 641–649 (2016).

7. Melvin, A. T., Welf, E. S., Wang, Y., Irvine, D. J. & Haugh, J. M. In chemotaxing fibroblasts, both high-fidelity and weakly biased cell movements track the localization of PI3K signaling. *Biophys J* **100,** 1893–1901 (2011).

8. Plotnikov, S. V. & Waterman, C. M. Guiding cell migration by tugging. *Curr Opin Cell Biol* **25,** 619–626 (2013).

9. McBeath, R., Pirone, D. M., Nelson, C. M., Bhadriraju, K. & Chen, C. S. Cell shape, cytoskeletal tension, and RhoA regulate stem cell lineage commitment. *Dev Cell* **6,** 483–495 (2004).

10. Wang, A. *et al.* Nonmuscle myosin II isoform and domain specificity during early mouse development. *Proc. Natl. Acad. Sci. U.S.A.* **107,** 14645–14650 (2010).

11. Müller, T. *et al.* Non-muscle myosin IIA is required for the development of the zebrafish glomerulus. *Kidney Int.* **80,** 1055–1063 (2011).

12. Schwarz, U. S. & Gardel, M. L. United we stand - integrating the actin cytoskeleton and cell-matrix adhesions in cellular mechanotransduction. *J Cell Sci* **125,** 3051–3060 (2012).

13. Blanchoin, L., Boujemaa-Paterski, R., Sykes, C. & Plastino, J. Actin dynamics, architecture, and mechanics in cell motility. *Physiol Rev* **94,** 235–263 (2014).

14. Fletcher, D. A. & Mullins, R. D. Cell mechanics and the cytoskeleton. *Nature* **463,** 485–492 (2010).

15. Hotulainen, P. & Lappalainen, P. Stress fibers are generated by two distinct actin assembly mechanisms in motile cells. *J Cell Biol* **173,** 383–394 (2006).

16. Devreotes, P. & Horwitz, A. R. Signaling Networks that Regulate Cell Migration. *Cold Spring Harb Perspect Biol* **7,** a005959 (2015).

17. Gardel, M. L., Schneider, I. C., Aratyn-Schaus, Y. & Waterman, C. M. Mechanical integration of actin and adhesion dynamics in cell migration. *Annu Rev Cell Dev Biol* **26,** 315–333 (2010).

18. Hoffman, B. D. & Crocker, J. C. Cell mechanics: dissecting the physical responses of cells to force. *Annu Rev Biomed Eng* **11,** 259–288 (2009).

19. Stricker, J., Falzone, T. & Gardel, M. L. Mechanics of the F-actin cytoskeleton. *J Biomech* **43,** 9–14 (2010).

20. Zhu, C., Bao, G. & Wang, N. Cell mechanics: mechanical response, cell adhesion, and molecular deformation. *Annu Rev Biomed Eng* **2,** 189–226 (2000).

21. Prost, J., Julicher, F. & Joanny, J.-F. Active gel physics. *Nature Physics* **11,** 111–117 (2015).

444   22.   Schwarz, U. S. & Safran, S. A. Physics of adherent cells. *Rev Mod Phys* **85,** 1327 (2013).

445   23.   Broedersz, C. P. & Mackintosh, F. C. Modeling semiflexible polymer networks. *Rev Mod Phys* **86,**
446   995 (2014).

447   24.   Ridley, A. J. & Hall, A. The small GTP-binding protein rho regulates the assembly of focal
448   adhesions and actin stress fibers in response to growth factors. *Cell* **70,** 389–399 (1992).

449   25.   Chrzanowska-Wodnicka, M. & Burridge, K. Rho-stimulated contractility drives the formation of
450   stress fibers and focal adhesions. *J Cell Biol* **133,** 1403–1415 (1996).

451   26.   Machacek, M. *et al.* Coordination of Rho GTPase activities during cell protrusion. *Nature* **461,**
452   99–103 (2009).

453   27.   Pertz, O., Hodgson, L., Klemke, R. L. & Hahn, K. M. Spatiotemporal dynamics of RhoA activity in
454   migrating cells. *Nature* **440,** 1069–1072 (2006).

455   28.   Strickland, D. *et al.* TULIPs: tunable, light-controlled interacting protein tags for cell biology. *Nat*
456   *Methods* **9,** 379–384 (2012).

457   29.   Guilluy, C. *et al.* The Rho GEFs LARG and GEF-H1 regulate the mechanical response to force on
458   integrins. *Nat Cell Biol* **13,** 722–727 (2011).

459   30.   Jaiswal, M. *et al.* Mechanistic insights into specificity, activity, and regulatory elements of the
460   regulator of G-protein signaling (RGS)-containing Rho-specific guanine nucleotide exchange
461   factors (GEFs) p115, PDZ-RhoGEF (PRG), and leukemia-associated RhoGEF (LARG). *J Biol Chem*
462   **286,** 18202–18212 (2011).

463   31.   Rizvi, S. A. *et al.* Identification and characterization of a small molecule inhibitor of formin-
464   mediated actin assembly. *Chem Biol* **16,** 1158–1168 (2009).

465   32.   Balaban, N. Q. *et al.* Force and focal adhesion assembly: a close relationship studied using elastic
466   micropatterned substrates. *Nat Cell Biol* **3,** 466–472 (2001).

467   33.   Sabass, B., Gardel, M., Waterman, C. M. & Schwarz, U. S. High resolution traction force
468   microscopy based on experimental and computational advances. *Biophys J* **94,** 207–220 (2008).

469   34.   Soiné, J. R. D. *et al.* Model-based Traction Force Microscopy Reveals Differential Tension in
470   Cellular Actin Bundles. *PLoS Comput Biol* **11,** e1004076 (2015).

471   35.   Oakes, P. W., Beckham, Y., Stricker, J. & Gardel, M. L. Tension is required but not sufficient for
472   focal adhesion maturation without a stress fiber template. *J Cell Biol* **196,** 363–374 (2012).

473   36.   Oakes, P. W., Banerjee, S., Marchetti, M. C. & Gardel, M. L. Geometry regulates traction stresses
474   in adherent cells. *Biophys J* **107,** 825–833 (2014).

475   37.   Ingber, D. E. Tensegrity I. Cell structure and hierarchical systems biology. *J Cell Sci* **116,** 1157–
476   1173 (2003).

477   38.   Webster, K. D., Ng, W. P. & Fletcher, D. A. Tensional Homeostasis in Single Fibroblasts. *Biophys J*
478   **107,** 146–155 (2014).

479   39.   Brox, T., Bruhn, A., Papenberg, N. & Weickert, J. in *Computer Vision - ECCV 2004* 25–36 (Springer
480   Berlin Heidelberg, 2004). doi:10.1007/978-3-540-24673-2_3

481   40.   Sánchez, J., Monzón, N. & Salgado, A. Robust Optical Flow Estimation. *Image Processing On Line*
482   **3,** 252–270 (2013).

483   41.   Cai, Y. *et al.* Cytoskeletal coherence requires myosin-IIA contractility. *J Cell Sci* **123,** 413–423
484   (2010).

485   42.   Xu, K., Babcock, H. P. & Zhuang, X. Dual-objective STORM reveals three-dimensional filament
486   organization in the actin cytoskeleton. *Nat Methods* **9,** 185–188 (2012).

487   43.   Colombelli, J. *et al.* Mechanosensing in actin stress fibers revealed by a close correlation

488   between force and protein localization. *J Cell Sci* **122,** 1665–1679 (2009).

489 44. Yoshigi, M., Hoffman, L. M., Jensen, C. C., Yost, H. J. & Beckerle, M. C. Mechanical force mobilizes
490   zyxin from focal adhesions to actin filaments and regulates cytoskeletal reinforcement. *J Cell Biol*
491   **171,** 209–215 (2005).

492 45. Zaidel-Bar, R., Ballestrem, C., Kam, Z. & Geiger, B. Early molecular events in the assembly of
493   matrix adhesions at the leading edge of migrating cells. *J Cell Sci* **116,** 4605–4613 (2003).

494 46. Smith, M. A. *et al.* LIM domains target actin regulators paxillin and zyxin to sites of stress fiber
495   strain. *PLoS ONE* **8,** e69378 (2013).

496 47. Smith, M. A., Hoffman, L. M. & Beckerle, M. C. LIM proteins in actin cytoskeleton
497   mechanoresponse. *Trends Cell Biol* **24,** 575–583 (2014).

498 48. Hoffman, L. M. *et al.* Genetic ablation of zyxin causes Mena/VASP mislocalization, increased
499   motility, and deficits in actin remodeling. *J Cell Biol* **172,** 771–782 (2006).

500 49. Smith, M. A. *et al.* A zyxin-mediated mechanism for actin stress fiber maintenance and repair.
501   *Dev Cell* **19,** 365–376 (2010).

502 50. Guo, W.-H. & Wang, Y.-L. Retrograde fluxes of focal adhesion proteins in response to cell
503   migration and mechanical signals. *Mol Biol Cell* **18,** 4519–4527 (2007).

504 51. Kanchanawong, P. *et al.* Nanoscale architecture of integrin-based cell adhesions. *Nature* **468,**
505   580–584 (2010).

506 52. Uemura, A., Nguyen, T.-N., Steele, A. N. & Yamada, S. The LIM domain of zyxin is sufficient for
507   force-induced accumulation of zyxin during cell migration. *Biophys J* **101,** 1069–1075 (2011).

508 53. Aratyn-Schaus, Y., Oakes, P. W. & Gardel, M. L. Dynamic and structural signatures of lamellar
509   actomyosin force generation. *Mol Biol Cell* **22,** 1330–1339 (2011).

510 54. Callan-Jones, A. C. & Voituriez, R. Active gel model of amoeboid cell motility. *New J Phys* **15,**
511   025022 (2013).

512 55. Besser, A. & Schwarz, U. S. Coupling biochemistry and mechanics in cell adhesion: a model for
513   inhomogeneous stress fiber contraction. *New J Phys* **9,** 425 (2007).

514 56. Edwards, C. M. & Schwarz, U. S. Force localization in contracting cell layers. *Phys Rev Lett* **107,**
515   128101 (2011).

516 57. Farsad, M. & Vernerey, F. J. An XFEM-based numerical strategy to model mechanical
517   interactions between biological cells and a deformable substrate. *Int J Numer Meth Engng* **92,**
518   238–267 (2012).

519 58. Weichsel, J., Urban, E., Small, J. V. & Schwarz, U. S. Reconstructing the orientation distribution of
520   actin filaments in the lamellipodium of migrating keratocytes from electron microscopy
521   tomography data. *Cytometry A* **81,** 496–507 (2012).

522 59. Butler, J. P., Tolić-Nørrelykke, I. M., Fabry, B. & Fredberg, J. J. Traction fields, moments, and
523   strain energy that cells exert on their surroundings. *Am J Physiol Cell Physiol* **282,** C595–605
524   (2002).

525

526

527   **Figure Captions**

528   **Figure 1**

529   RhoA activity can be spatiotemporally controlled via an optogenetic probe. (**a**) Spatiotemporal control

530   of RhoA activity is achieved using an optogenetic probe to recruit the RhoA specific GEF LARG to the

531   plasma membrane. A LOVpep molecule is anchored to the membrane via fusion to the transmembrane

532   protein Stargazin, while a protein consisting of tandem PDZ domains fused to the DH domain of LARG

533   (prGEF) is distributed throughout the cytosol. Upon stimulation with 405nm light, the LOVpep

534   undergoes a conformational change exposing a high-affinity binding site which drives the prGEF to the

535   membrane where it can activate RhoA. When the activating light is removed, the LOVpep undergoes a

536   thermodynamically driven refolding halting further recruitment of prGEF. (**b**) The RhoA signaling

537   pathway. RhoA*GTP activates both Dia and ROCK, which in turn promote actin polymerization and

538   myosin II activation, respectively. (**c**) Representative images of a 3T3 fibroblast expressing an mCherry-

539   tagged version of prGEF. Upon local activation (top row – orange box) mCherry-prGEF rapidly

540   accumulates in the activation region. Removal of the activating light (bottom row) results in the

541   accumulated mCherry-prGEF dispersing back into the cytosol. (**d**) Quantification of the local intensity

542   increase of mCherry-prGEF in the activation region of the cell shown in **c**. The activation period is

543   indicated by a blue background. (**e-f**) Representative images of cells expressing either mApple-Actin (**e**)

544   or mApple-Myosin Light Chain (**f**) prior to activation, following 15 minutes of activation in the region

545   indicated, and following 15 minutes of relaxation. Both actin and myosin exhibit increases in intensity

546   in the local region of activation. (**g**) Quantification of the local intensity increase of actin and myosin

547   from the cells in **e-f**. Both signals begin increasing immediately upon RhoA activation, and dissipate as

548   soon as the activating light is switched off. (**h**) Mean maximum intensity fold-increase of actin or

549   myosin in regions of activation in control cells, or cells treated with 10 µM SMIFH2 (Dia inhibitor) or

550   1µM Y-27632 (ROCK inhibitor). Inhibition of either Dia or ROCK results in reduced average increases in

551   local intensity during RhoA activation. Time is min:sec.

552

553   **Figure 2**

554   Increased RhoA activity leads to increased cell contractility. (**a**) A cell expressing mCherry-Vinculin is

555   shown prior to activation, after 15 minutes of activation, and after 15 minutes of relaxation. The

20

556   activation region is indicated by the orange box. (**b**) The corresponding traction stress maps for the

557   time series shown in **a**. (**c**) A plot showing the strain energy versus time and the number of focal

558   adhesions versus time, with the activation period indicated by the blue background. The strain energy

559   begins to increase immediately upon activation, and begins to relax as soon as the activating light is

560   removed. In contrast, the number of focal adhesions remains relatively constant and does not respond

561   to the local increase in RhoA activity. (**d**) The average stress and fluorescence intensity of a

562   representative adhesion marked by the white box in **a**. Kymographs were generated by drawing a line

563   along the long axis of the adhesion. The activation period is indicated by the orange bar above the

564   kymograph. (**e**) A sequence of traction maps from a cell exposed to a series of activations in regions of

565   different size. Time is hr:min:sec. (**f**) A plot of the experimental (black line) and theoretical (red line)

566   strain energy vs time for the cell shown in **e**. The contractile response of the cell is proportional to the

567   size of the activation region and retreats to a baseline value following each activation period. (**g**) A

568   cartoon of the continuum model used to describe the cell in **e**. The model consists of a contractile

569   element (σ_m) in series with a viscous (η) and an elastic element (k), connected via a frictional elements

570   (γ) to an elastic substrate (k_M).

571

572   **Figure 3**

573   Stress fibers direct contractile flow. (**a**) Fluorescence time series of a cell expressing mApple-MLC

574   shown prior and after two separate periods of activation (orange boxes). (**b**) Flow fields of myosin

575   calculated from the images in **a**. Flow is always directed along the direction of the stress fibers. (**c**) A

576   two dimensional model of the cell was created using a triangular mesh of viscoelastic-cables (k, η)

577   connected at vertices viscously coupled (γ) to the environment. Stress fibers (blue line) consisting of

578   contractile (σ_m), viscous (η_{SF}) and elastic elements (k_{SF}) were embedded in the network. Using a

579   simplified rectangular cell with this network, local RhoA activation could be simulated by activating

580   force dipoles in network links in a region in the center of the cell. (**d**) To calibrate the 2D discrete

581   model, the average flow (white box in **c**), was measured and compared to the 1D continuum model

582   presented above. (**e-f**) The 2D discrete model was used to explore two contractile scenarios: (**e**)

583   contractile stress fibers (blue) embedded in a contractile mesh (grey); and (**f**) contractile stress fibers

584   embedded in a non-contractile background. If both the stress fibers and mesh are contractile, a

585   transverse contraction pinches together the stress fibers. If only the stress fibers contract, the flow

586   profile is restricted to the orientation of the fibers, mimicking the experimental results.

587

588   **Figure 4**

589   Stress fibers behave elastically. (**a**) Image showing a cell labeled with mApple-MLC. The activation

590   regions are indicated by the orange boxes. (**b**) A kymograph drawn along the stress fiber (green line in

591   **a**). During activation periods myosin flows towards the activation regions. (**c**) A kymograph created

592   from the same region as **b** using the flow maps determined previously. Flow was projected onto the

593   stress fiber and color coded to indicate speed and direction. This flow map illustrates that during

594   relaxation periods, myosin flow reverses direction away from the activation periods. (**d**) A

595   quantification of displacement of stress fibers during contraction and relaxation. Puncta ~5 μm from

596   the activation zone were tracked and measured following 15 minutes of activation, and again following

597   15 min of relaxation. Puncta translated about 3 μm from their original position, and relaxed to ~1 μm

598   from their original position elastically. The relaxation response could be further broken into two

599   groups, one with a strong reversal (~80% of their original position) and one with a weak reversal (~25%

600   of their original position). (**e**) A cell transfected with mApple-α-actinin. The activation area is indicated

601   by the orange box. (**f**) A kymograph drawn along the direction indicated in **e**, overlain with tracks of the

602   individual α-actinin puncta during activation. (**g**) The velocity of individual puncta along the stress fiber

603   is measured from the slope of the tracks and plotted against the distance from the activation region.

604   Adjacent puncta all move at approximately the same speed. Sudden changes in velocity (blue

605   arrowhead) correlate with what appear to be site of mechanical failure along the stress fiber and the

606   appearance of new puncta. The black line represents the stress fiber from **f**, while the grey lines are

607   other stress fibers from the same cell. (**h**) A representative kymograph is fit to both the 1D continuum

608   and 2D discrete models. Both models are able to recapitulate the flow patterns seen experimentally.

609

610   **Figure 5**

611   Zyxin accumulates at sites of strain on stress fibers during local RhoA activation. (**a**) A NIH 3T3

612   expressing mCherry-zyxin. The activation region is indicated by the orange box. (**b**) A kymograph of a

613   representative adhesion marked by the white box in **a**. (**c**) The average intensity of zyxin in the

614   activation region. (**d**) A kymograph illustrating the local zyxin accumulation during activation along the

615   green line shown in **a**. (**e**) A zyxin$^{(-/-)}$ MEF expressing mApple-MLC before activation, at peak activation,

616   and following relaxation. Myosin accumulates as in 3T3s. (**f**) A kymograph of myosin intensity and flow

617   speed drawn along the green line indicated in **e**. Zyxin$^{(-/-)}$ MEFS exhibit little to no elastic flow reversal.

618   (**g**) A zyxin$^{(-/-)}$ MEF rescued with EGFP-zyxin and expressing mApple-MLC, during an activation

619   sequence. (**h**) A kymograph of myosin and flow illustrating a strong elastic flow reversal along the line

620   drawn in **g**. (**i**) Displacement analysis of the zyxin$^{(-/-)}$ and zyxin$^{(-/-)}$+EGFP-zyxin MEFs. Without zyxin, cells

621   do not exhibit an elastic response. (**j**) A kymograph representing the average fit of the continuum

622   model to the zyxin$^{(-/-)}$ data. (**k**) A kymograph representing the average fit of the continuum model to

623   the zyxin$^{(-/-)}$+EGFP-zyxin data. (**l**) The elastic (E) and viscous (η) parameters found from fitting the

624   experimental kymographs to the continuum model. Without zyxin, the elasticity increases and the

625   viscosity decreases.

626

627   **Figure 6**

628   Molecular and mechanical models of local RhoA activation in stress fibers. Molecular model: (1) Local

629   recruitment of prGEF leads to activation of RhoA and accumulation of actin and myosin. The local

630   increase in actin and myosin in turn stimulates a local contraction in the stress fiber. (2) The increased

631   local contractility induces a flow of myosin and α-actinin along the stress fiber towards the activation

632   region. (3) Increased flow induces higher strain at both the interface coupling the stress fiber to the

633   focal adhesion and the activation region, resulting in recruitment of the mechanosensitive protein

634   zyxin. (4) When local activation of RhoA stops, the flow reverses direction as the stress fiber relaxes

635   elastically. Mechanical model: The stress fiber is represented as a contractile, viscous and elastic

636   element connected in series. Upon local activation of RhoA, the contractile element is compressed,

637   leading to extension of both the viscous and elastic elements. As local activation stops, the energy

638   stored in the elastic element allows it to relax back to its original state, while the energy in the viscous

639   element is lost.

640

641

Supplementary Movie Captions

Supplementary Movie 1

A NIH 3T3 fibroblast expressing mCherry-prGEF during a local activation of RhoA (from Figure 1c). Local activation area is indicated by the white box. Time is in min:sec.

Supplementary Movie 2

A NIH 3T3 fibroblast expressing mApple-Actin during local activation of RhoA (from Figure 1e). Local activation area is indicated by the white box. Time is in min:sec.

Supplementary Movie 3

A NIH 3T3 fibroblast expressing mApple-MLC during a local activation of RhoA (from Figure 1f). Local activation area is indicated by the white box. Time is in min:sec.

Supplementary Movie 4

A NIH 3T3 fibroblast expressing mCherry-vinculin during a local activation of RhoA (from Figure 2a) and the corresponding traction stress maps (from Figure 2b). Local activation is indicated by the white box. Time is in min:sec.

Supplementary Movie 5

Traction stress maps of a NIH 3T3 fibroblast during a series of local RhoA activations (from Figure 2e). Local activation is indicated by white boxes. Time is in hr:min:sec.

Supplementary Movie 6

A NIH 3T3 fibroblast expressing mApple-MLC during a local activation of RhoA and the corresponding cytoskeletal flow maps (from Figure 3a,b). Local activation is indicated by white boxes. Time is in hr:min:sec.

671 **Supplementary Movie 7**

672 A NIH 3T3 fibroblast expressing mApple-MLC during 3 sequential local activations of RhoA. Each

673 activation is the same area but of a different geometry. Local activation is indicated by white boxes.

674 Time is in hr:min:sec.

675

676 **Supplementary Movie 8**

677 A NIH 3T3 fibroblast expressing mApple-α-actinin during a local activation of RhoA (from Figure 4e).

678 Local activation is indicated by white boxes. Time is in min:sec.

679

680 **Supplementary Movie 9**

681 A NIH 3T3 fibroblast expressing mCherry-Zyxin during a local activation of RhoA (from Figure 5a). Local

682 activation is indicated by white boxes. Time is in min:sec.

683

684 **Supplementary Movie 10**

685 A zyxin[(-/-)] Mouse Embryonic Fibroblast expressing mApple-MLC during a local activation of RhoA (from

686 Figure 5e). Local activation is indicated by white boxes. Time is in min:sec.

687

688 **Supplementary Movie 11**

689 A zyxin[(-/-)]+EGFP-zyxin Mouse Embryonic Fibroblast expressing mApple-MLC during a local activation of

690 RhoA (from Figure 5g). Local activation is indicated by white boxes. Time is in min:sec.
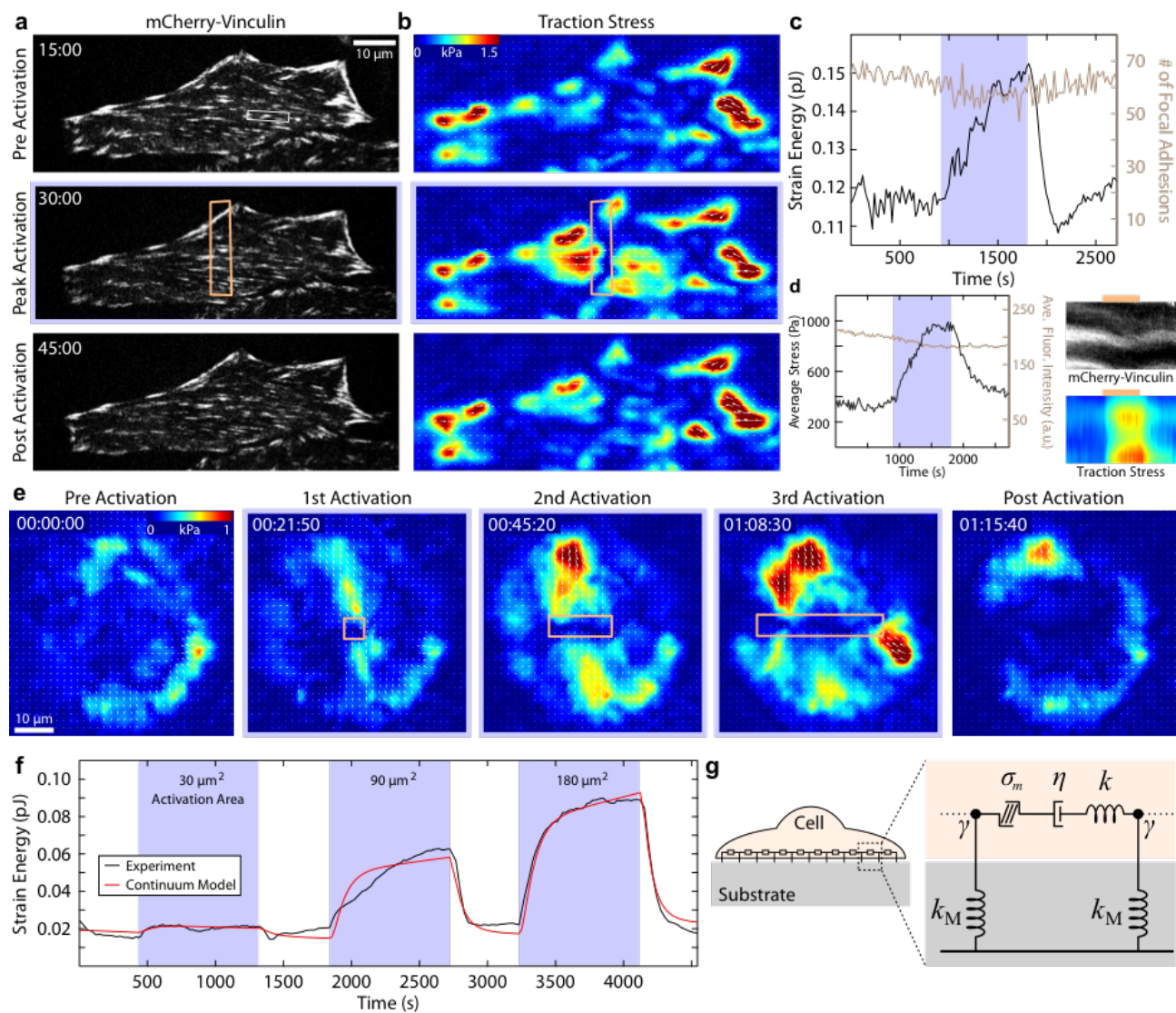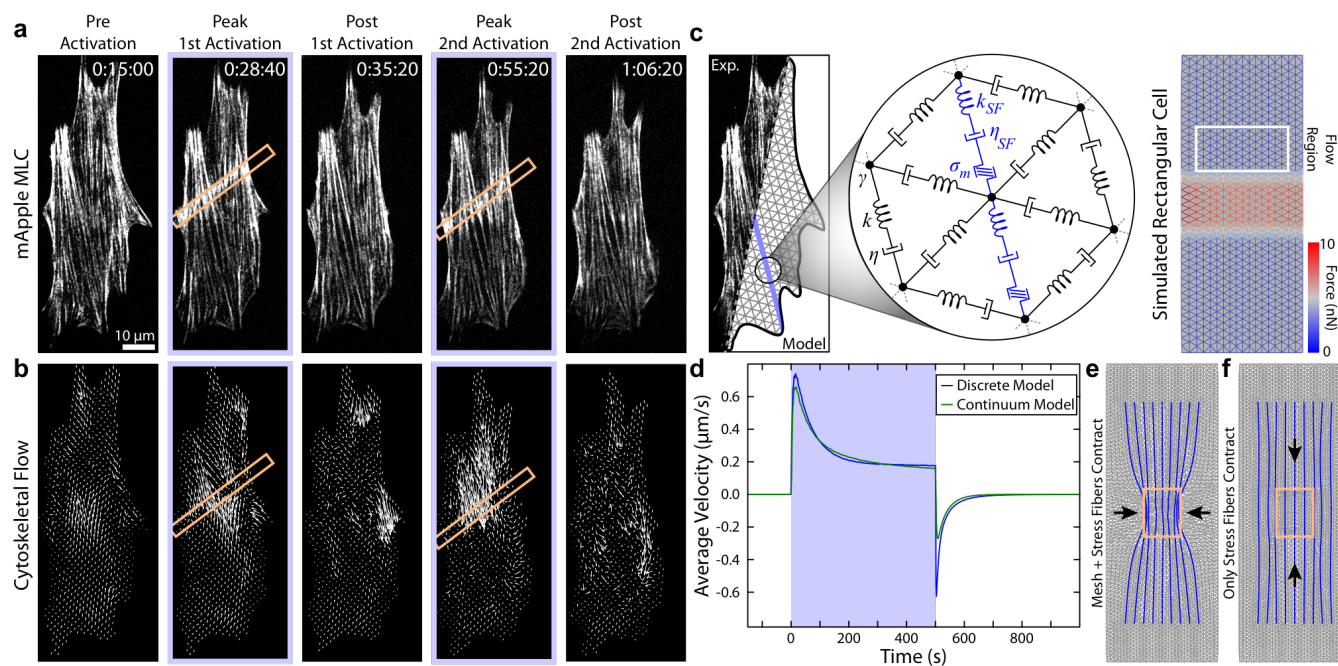
691
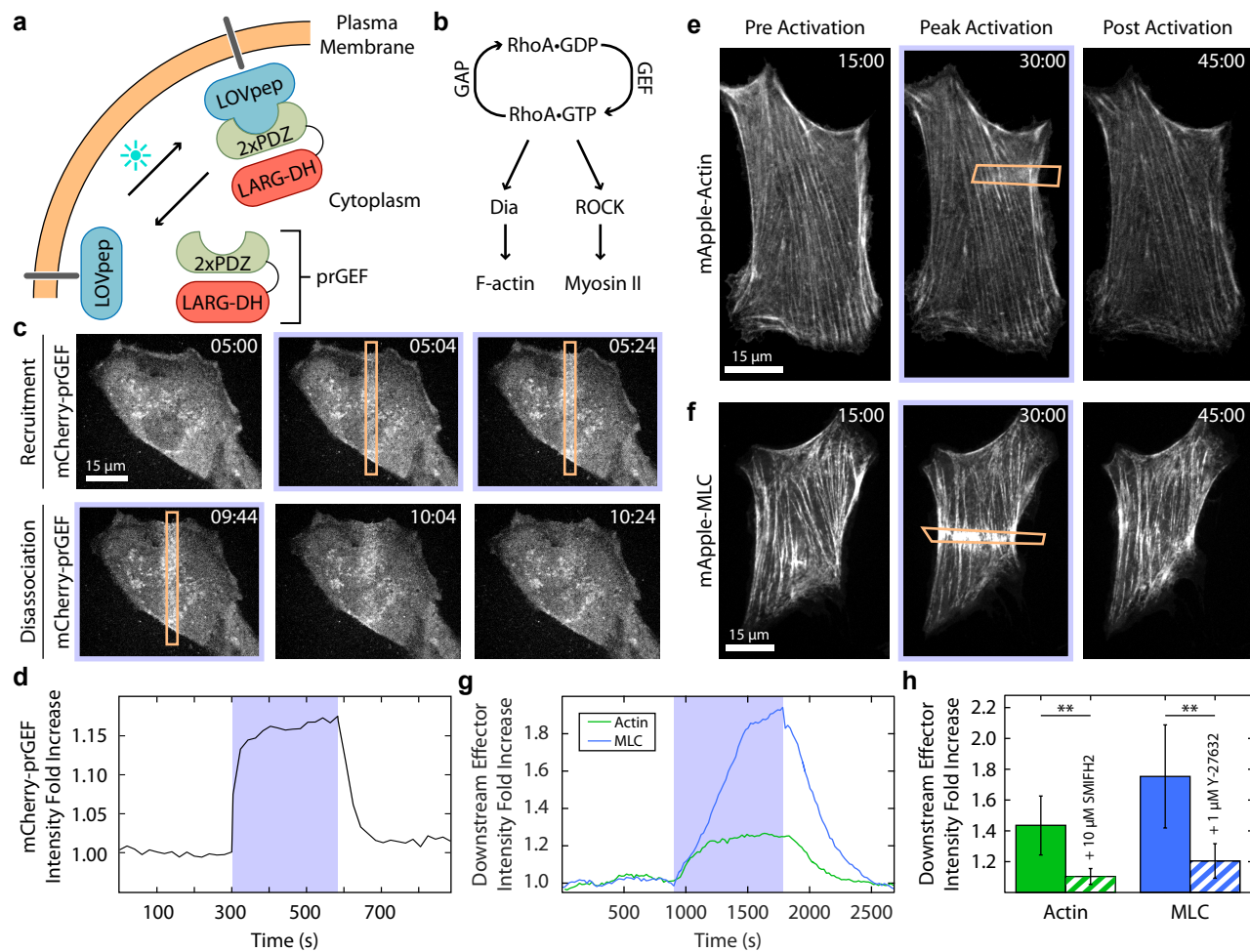
Figure 1

695 **Figure 2**

696

697

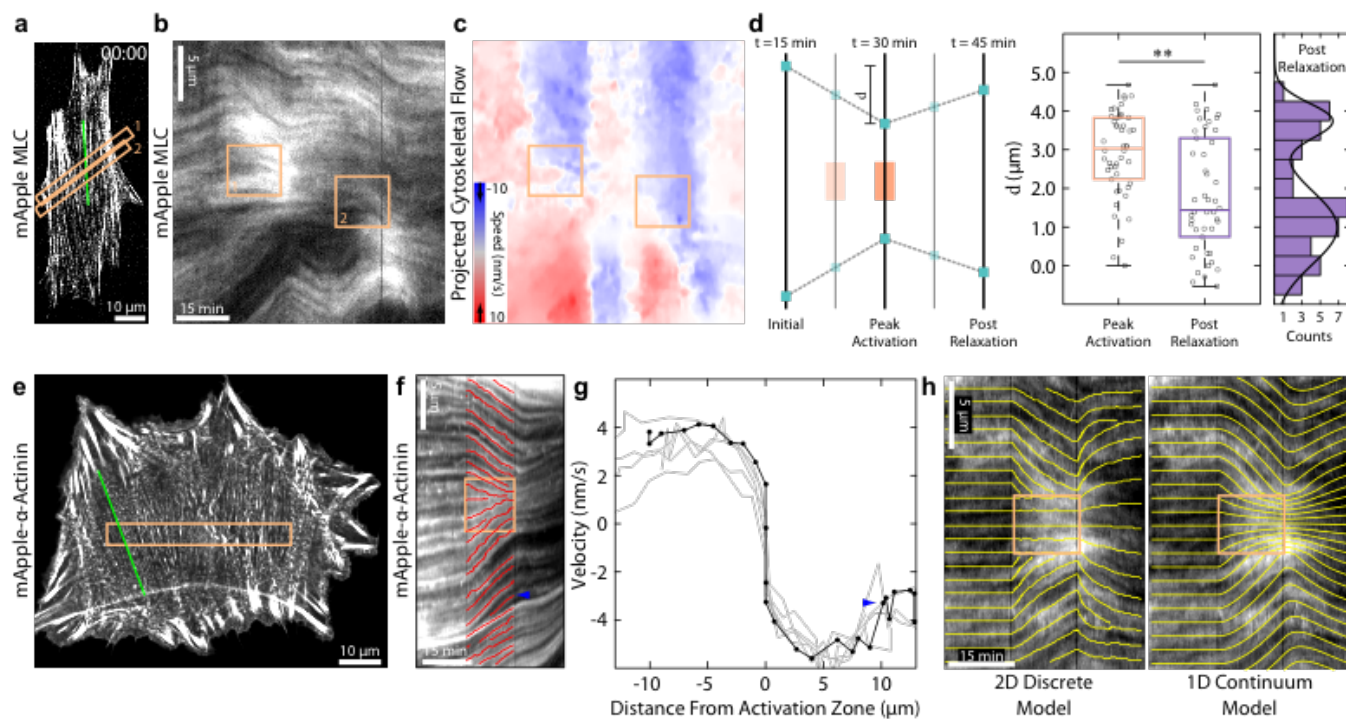698   **Figure 3**

699

700

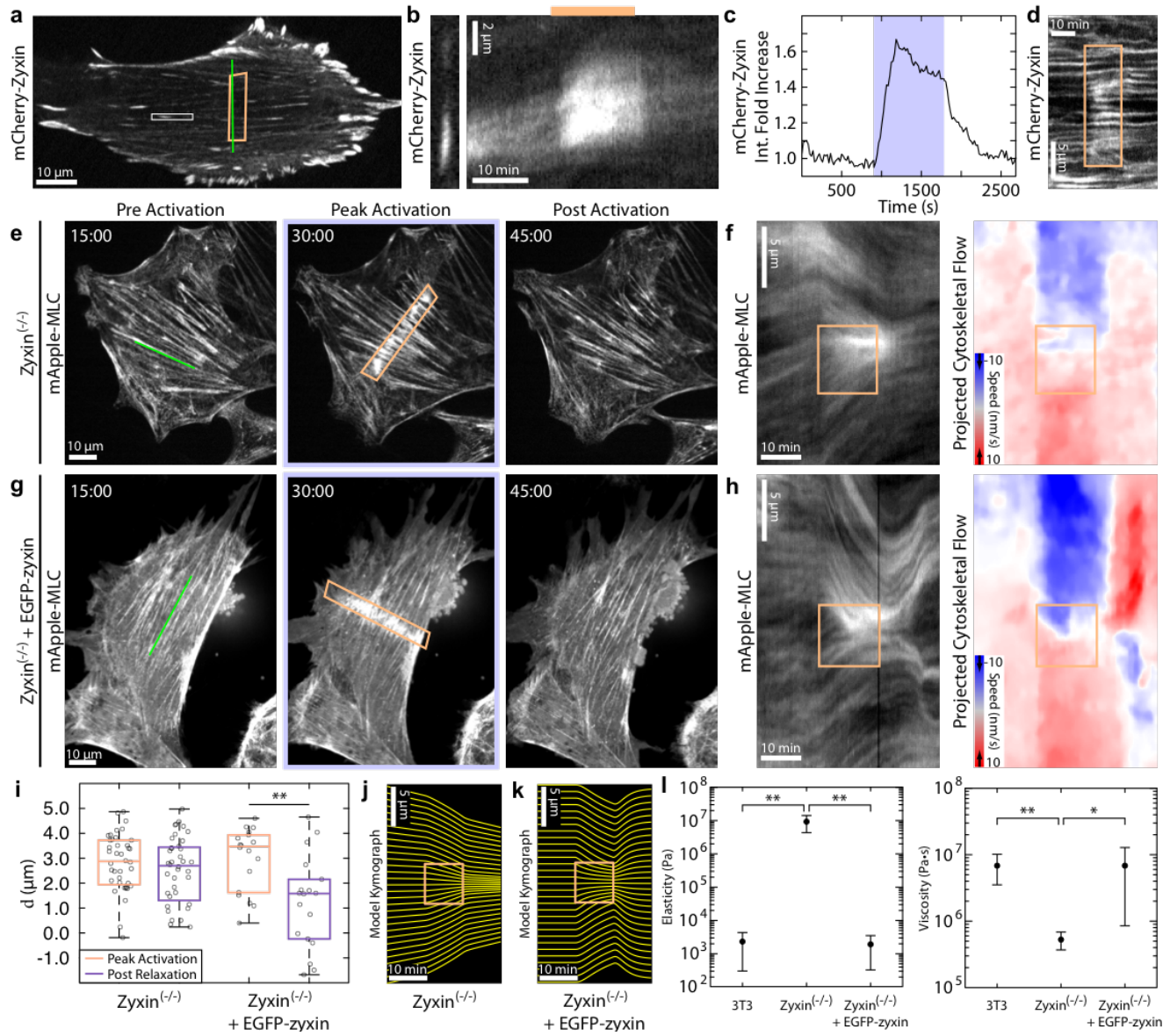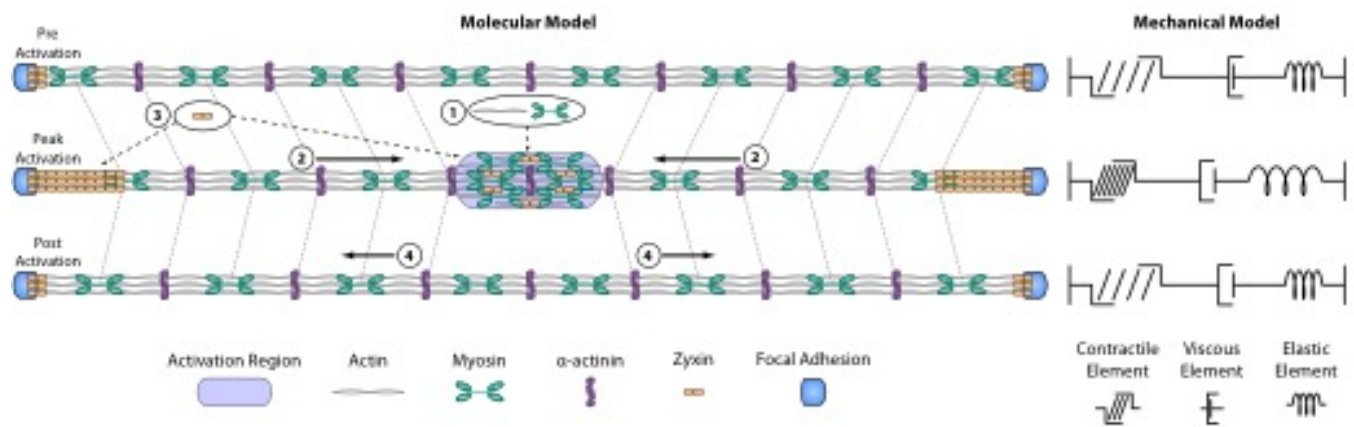701   **Figure 4**

702

703

704   **Figure 5**

705

706

707 **Figure 6**